*Korean J. Chem. Eng.*, 34(9), 2480-2487 (2017)
DOI: 10.1007/s11814-017-0145-7

pISSN: 0256-1115
eISSN: 1975-7220

# Effect of functionalized multiwalled carbon nanotubes on weather degradation and corrosion of waterborne polyurethane coatings

**Mohammad Mizanur Rahman*,†, Rami Suleiman*, and Han Do Kim****

*Center of Research Excellence in Corrosion, King Fahd University of Petroleum & Minerals Dhahran 31261, Kingdom of Saudi Arabia
**Department of Organic Material Science and Engineering, Pusan National University, Busan 46239, Korea
(*Received 10 January 2017 • accepted 24 May 2017*)

**Abstract**−A series of waterborne polyurethane/functionalized multiwalled carbon nanotube (WBPU/*f*-MWCNT) nanocomposite dispersions was prepared using three defined concentrations of 0.5, 1.0 and 2.0 wt% carboxyl functionalized multiwalled carbon nanotubes (*f*-MWCNTs). All dispersions were coated on mild steel and exposed under natural weather condition for a maximum of 365 days. Both exposed and unexposed coatings were characterized by potentiodynamic polarization (PDP) and X-ray photoelectron spectroscopy (XPS) analyses. The pristine WBPU coating showed slight degradation and corrosion protection. Inclusion of a higher content of *f*-MWCNTs significantly improved both the degradation and corrosion protection efficiencies of the coatings. Maximal degradation and corrosion protection was observed when 2.0 wt% *f*-MWCNT was mixed with WBPU for all of the coatings.

Keywords: Polyurethane, Corrosion, MWCNT

## INTRODUCTION

Polyurethane (PU) holds a unique position in the coating industry because of its excellent mechanical strength, adhesive strength, thermal stability and barrier resistance. PU consists of two segments: a soft segment and a hard segment. The soft segment is commonly composed of a polyester or polyether polyol, whereas the hard segment consists of a low molecular weight diol or diamine reacted with diisocyanate [1,2]. By changing the soft and hard segments and their ratio, the properties can be tuned and applied to many different applications. PU can be classified as either solventborne or waterborne based on the solvent system during synthesis. Solventborne PU is restricted because of the emission of toxic solvent. However, waterborne polyurethane (WBPU) emits mainly water and is considered an environmentally friendly coating [3-5].

The main environmental factors that cause weather degradation, resulting in corrosion of organic coatings, are ultraviolet (uv) radiation, oxygen and water [6,7]. To reduce degradation from UV radiation, UV absorbers are often incorporated into coatings. Both organic and inorganic absorbers are used to minimize degradation; however, both have limitations. Organic absorbers suffer from migration and degradation over time, which limits their long-term stability in coatings. Inorganic absorbers suffer mainly from agglomerates and the tendency to migrate to bulk coating at high loadings [8-10]. Recently, nano materials have shown some promising results in this regard [10-12].

Typically, the properties of polymer coatings are analyzed in the lab under ambient conditions. Only few researchers have considered artificial harsh weather conditions for analysis [13,14]. Rahman et al. [13] studied the effect of dimethylolpropionic acid (DMPA) and CNT content on the adhesive strength of the polyether-based WBPU. The WBPU materials were used to adhered nylon fabrics. The resistivity of this adhesive material was checked by applying different defined temperatures. The adhesive strength increased with inclusion of CNT at room temperature. However, the adhesive strength gradually decreased with increasing temperature. Rahman and Kim [14] also found that the adhesive strength also depends on polyol. They used different polyols [polyester polyols ($M_n$= 2000), namely poly(tetramethylene adipate glycol) (PTAd) and poly(caprolactone glycol) (PCL), and polyether polyols ($M_n$=2000), namely poly(tetramethylene oxide glycol) (PTMG) and poly(propylene glycol) (PPG)] in WBPU adhesive material. Poly(tetramethylene adipate glycol) based WBPU showed a good adhesive strength even at moderate high temperature of 100 °C. However, from a practical point of view, the coating properties are also subjected to typical environmental stresses, such as high temperature, high humidity and UV radiation. All of these factors can also induce coating degradation, which eventually induces metal corrosion. Therefore, it is important to characterize the coatings after long exposure under harsh conditions to avoid unusual behaviors when applied in real practical fields.

Inhibiting the corrosion of metals is a critical part of the gas and oil pipeline industry, which can be achieved by selecting proper materials, using an external inhibitor or applying a coating [15-17]. The gas and oil pipeline industry has been facing tough challenges because the most successful chromate-based coating has been banned in accordance with environmental legislation [18,19]. In the past decade, several environmentally friendly efforts have been reported as a replacement for chromate-based coatings. Metroke et al. examined silane coatings [19-22], which were found to im-

†To whom correspondence should be addressed.
E-mail: mrahman@kfupm.edu.sa

prove corrosion resistance when the alkyl-silane reached a certain value in the coating. Voevodin et al. found that a cerium-doped, zirconium-epoxy sol-gel coating provided good corrosion inhibition [23]. Kinlen et al. reported a polyaniline, which can passivate exposed metal areas, such as scratches and pinholes [24]. Markevicius et al. examined copolymers of polyurethane-polyoligomeric silsesquioxane coatings [25].

In the coating industry, carbon nanotube (CNT) nanocomposites are being considered as promising candidates, because of their extraordinary mechanical properties, thermal stability and superior conducting properties. Over the last decade, MWCNTs and functionalized MWCNTs have been used in different polymers, such as epoxy, acrylate and polyurethane. A homogeneous dispersion of functionalized multiwalled carbon nanotubes (*f*-MWCNTs) in those polymers has already been shown to significantly improve their mechanical, thermal, barrier and adhesive strengths [26-29]. These properties can be further improved by choosing proper monomers and balancing their contents, as well as increasing the content of dispersed homogeneous *f*-MWCNTs. However, no studies have considered the use of *f*-MWCNTs to protect the coating from natural weather degradation, which would lead to a reduction in corrosion. In this report, WBPU/*f*-MWCNT coatings were prepared using three defined concentrations (0.5, 1.0, and 2.0 wt%) of *f*-MWCNTs. Kwon and Kim [30] used functionalized and non-functionalized MWCNT in WBPU material. They compared the thermal and mechanical properties of WBPU/MWCNT materials based on their functionality. This has been confirmed as better improvement of properties using *f*-MWCNTs than pristine *f*-MWCNTs. Therefore, in this study only *f*-MWCNTs were considered to improve the degradation and corrosion properties of WBPU coatings. Mild steel was used as a substrate and the coated samples were exposed to natural weather conditions for 365 days. The visual inspection was analyzed in the lab using potentiodynamic polarization (PDP) and XPS techniques. XPS was also used to analyze the degradation of the exposed coatings.

## EXPERIMENTAL

### 1. Materials

Poly(tetramethyleneoxide glycol), (PTMG Mn=2000, Sigma Aldrich) and poly(ethylene glycol), (PEG Mn=400, Sigma Aldrich) were vacuum dried at 90 °C for three hours prior to use. Dimethylolpropionic acid (DMPA, 98%, Sigma Aldrich), triethylamine (TEA, ≥99%, Sigma Aldrich), *N*-methyl-2-pyrrolidone (NMP, 99.5%, Sigma Aldrich), 4,4-dicyclohexylmethane diisocyanate ($H_{12}$MDI, Sigma Aldrich) and ethylene diamine (EDA, ≥99.5%, Sigma Aldrich) were used after dehydration with 4 Å molecular sieves for seven days. Pristine MWCNTs were functionalized as in a previous report [13]. Dibutyltindilaurate (DBTDL, 95%, Sigma Aldrich) was used as received.

### 2. Functionalization of MWCNTs

The raw MWCNTs were washed with 20% hydrofluoric acid for 5 h and 22% nitric acid for a period of 10 h and then subsequently washed with distilled water. The washed MWCNTs were treated with boiled concentric nitric acid for a period of 0.5 h, and the MWCNTs were washed with distilled water and acetone.

### 3. Preparation of WBPU Dispersion

A prepolymer mixing method was applied for the synthesis of a pristine WBPU dispersion [14]. The NCO-terminated prepolymer was obtained by reacting PTMG, PEG, DMPA and $H_{12}$MDI along with DBTDL as a catalyst. The prepolymer mixture was then mixed with 10 wt% methyl ethylketone to maintain its viscosity. The carboxyl group of the NCO-terminated prepolymer was then neutralized using TEA. Distilled water (calculated 70 wt%) was added to the reaction mixture after 30 minutes of neutralization under intense stirring. EDA (mixed with water, 1 g: 10 g) was added to the mixture to induce chain extension of the pre-polymer. WBPU dispersions (30 wt% solid content) were obtained after evaporation of MEK. The solid content was determined through the following calculation:

$$\text{Solid content} = \frac{\text{Dry content}}{\text{Wet content}} \times 100\%$$

### 4. Preparation of WBPU/*f*-MWCNT Nanocomposite Dispersion

WBPU/*f*-MWCNT nanocomposite dispersions were formed via a physical intermixing process. Three defined concentrations of *f*-MWCNTs (0.5, 1 and 2 wt%) were mixed with water using ultrasonication for 10 minutes. In another vessel, the prepolymer was prepared by the same procedure as the pristine WBPU. The *f*-MWCNTs/water mixture was added at the dispersion step. The WBPU/*f*-MWCNT dispersion was chain-extended by dropping an EDA/$H_2O$ mixture at 40 °C for 1 h, and the reaction continued until the NCO peak (2,270 $cm^{-1}$) in the IR spectrum had completely disappeared. After evaporation of MEK, the WBPU/*f*-MWCNT nanocomposite dispersions were obtained.

### 5. Coating Preparation

The coatings were prepared on the mild steel substrate by using a control coater which can make the wet coating as a controlled way. The surface of the steel substrate was cleaned with acetone prior to coating. A constant wet thickness of 100 μm was maintained for all the coatings. Then, the coatings were dried in an oven at 60 °C. The coated mild steel plate samples were placed on a rooftop in open atmosphere under the natural climatic conditions of the

**Table 1. Temperature and humidity during the exposure time**

| Temperature °C/ Humidity (%) | August | September | October | November | December | January | February | March | April | May | June | July |
|---|---|---|---|---|---|---|---|---|---|---|---|---|
| Average high temperature | 41 | 38 | 34 | 27 | 22 | 19 | 21 | 25 | 31 | 37 | 40 | 42 |
| Average low temperature | 28 | 25 | 21 | 17 | 12 | 10 | 11 | 15 | 20 | 24 | 27 | 28 |
| Average temperature | 35 | 32 | 28 | 22 | 17 | 15 | 16 | 20 | 25 | 31 | 34 | 35 |
| Average relative humidity | 45 | 50 | 60 | 65 | 70 | 70 | 65 | 55 | 45 | 35 | 35 | 35 |

Kingdom of Saudi Arabia. The recorded temperature (°C) and relative humidity (%) during the exposure time are summarized in Table 1. The coatings were exposed from August 1st, 2012 to July 30th, 2013. Photographs of the coatings were taken at regular intervals using a high-resolution camera to monitor the corrosion progress on the steel substrate.

**6. Characterization**

FTIR spectroscopy (Impact 400D, Nicolet, Madison, WI) was used to identify the WBPU film structure. The dispersion was coated on a thallium bromide/thallium iodide crystal surface as a thin liquid film and dried for analysis. For each sample, 32 scans at a resolution of 4 $cm^{-1}$ were collected in transmittance mode.

A Hitachi model H-7500 transmission electron microscope (TEM) was used to examine the morphology of the coatings. The samples for TEM analysis were prepared by placing the nanocomposite films in epoxy capsules and curing the epoxy at 70 °C for 24 h in an oven. The cured epoxies containing the WBPU/*f*-MWCNT nanocomposite films were then microtomed with a diamond knife into 70-90-nm-thick slices at −100 °C. Finally, a 3-nm-thick carbon layer was deposited on the slices for TEM observation.

For the water absorption study, all films were immersed in water for 48 h at 30 °C and the water absorption (%) was determined from the weight increase as:

$$\text{Swelling (\%)} = \frac{W - W_0}{W_0} \times 100$$

where $W_0$ is the weight of the dried film and W is the weight of the film at equilibrium swelling.

Water contact angle measurements were performed using a Theata Optical tensiometer (Attension, Finland). An automatic single liquid dispenser was used to automatically dispense a precise volume of water drop (5 μL), which then descended until the drop contacted the coating. An image of the water drop, taken by a camera on the instrument, was analyzed by Attension software to obtain the water contact angles. The value is the average of 5 runs.

Potentiodynamic polarization (PDP) analysis was performed using a GAMRY3000 corrosion measurement system (potentiostat). The potential of the electrode was varied from –0.2 V to 0.2 V. The electrochemical cell used for the current study consisted of the prepared coated electrode as the working electrode, a graphite rod as the counter electrode, an SCE as the reference electrode, and 3.5 wt% sodium chloride as the electrolyte. EChem Analyst software package 6.0 was used for all the analyses, curve extrapolation, fitting and simulations of PDP data. A surface mask (GAMRY) with an area of 1 $cm^2$ was used to mask the analyzed surface.

The polymer surface was analyzed by X-ray photoelectron spectroscopy (XPS) (ESCA 250 XPS, UK) using a monochromated Al K$\alpha$ X-ray source (15 kV, 25 W) and a spot size 400×400 μm. The spectra were then analyzed, employing a curve fitting technique based on a linear least-squares analysis to fit a combination of the Lorentzian and Gaussian curve shapes.

## RESULTS AND DISCUSSION

Raman scattering is a powerful technique to characterize the

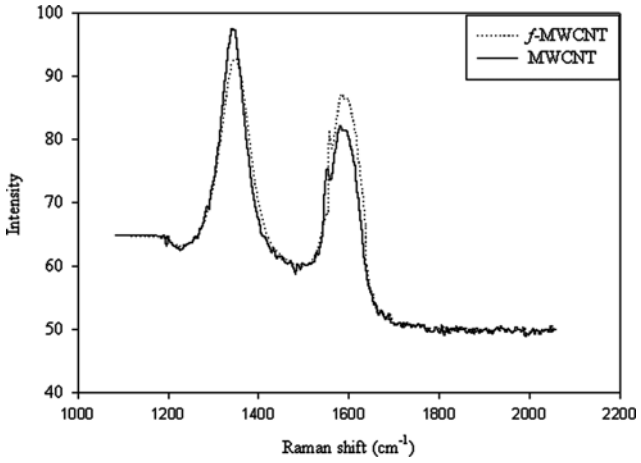


**Fig. 1. Raman scattering spectra of MWCNT and *f*-MWCNT.**

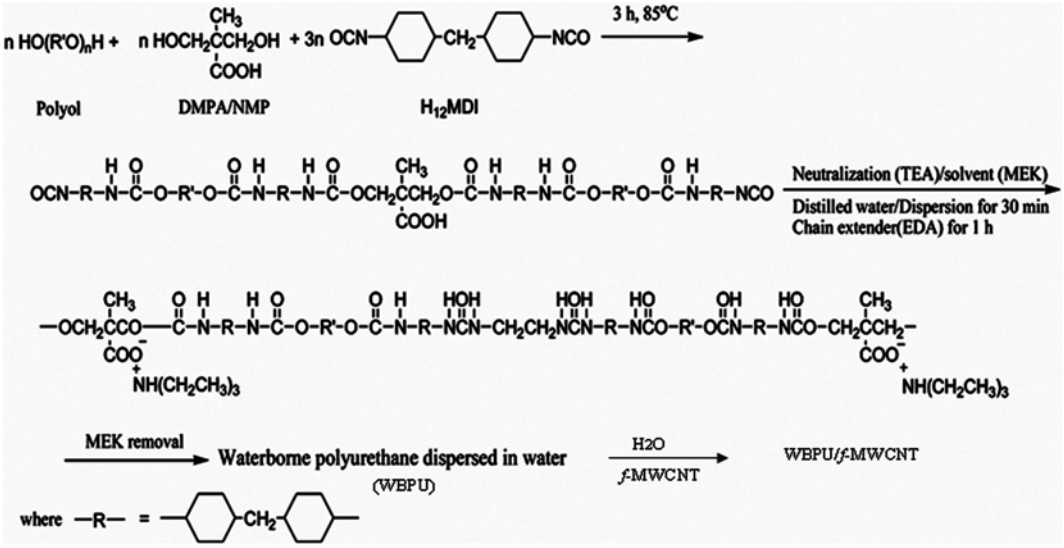


**Scheme 1. Preparation of WBPU/*f*-MWCNT dispersion.**

**Table 2. Sample designation and composition of WBPU/*f*MWCNT coatings**

| Sample designation | Composition (molar ratio) | | | | | *f*-MWCNT (wt%) |
|---|---|---|---|---|---|---|
| | DMPA | PTMG/PEG | $H_{12}$MDI | EDA | TEA | |
| WBPU | 0.074 | 0.04 | 0.134 | 0.014 | 0.074 | 0 |
| WBPU/*f*-MWCNT-1 | 0.074 | 0.04 | 0.134 | 0.014 | 0.074 | 0.5 |
| WBPU/*f*-MWCNT-2 | 0.074 | 0.04 | 0.134 | 0.014 | 0.074 | 1.0 |
| WBPU/*f*-MWCNT-3 | 0.074 | 0.04 | 0.134 | 0.014 | 0.074 | 2.0 |

pristine MWCNT and *f*-MWCNT. Fig. 1 shows the typical Raman spectra of MWCNT and *f*-MWCNT. Two strong scattering peaks were observed for both MWCNT and *f*-MWCNT centered at 1,341 and 1,583/cm, respectively. The band centered at 1,583/cm was assigned to the graphite-like tangential mode "G" band, and the so-called "D" band centered at 1,341/cm was attributed to disorder or to sp3-hybridized carbon in the hexagonal framework of the nanotube walls. The intensity ratio of the band at ~1,583/cm to that at 1341/cm (G to D) reflects the proportion and purity of the MWCNT in the samples [31]. Although the shape and positions of peaks in the spectra are fairly similar to each other, the value of the G-to-D ratio displayed some regular and substantial changes, which can reveal something about the structural information of the sample. The increase in the relative intensity of the disordered mode can be attributed to the increased number of structural defects and to the sp3 hybridization of carbon for chemically induced disruption of the hexagonal carbon order in the nanotubes after acid treatment. This may be due to the attachment of carboxylic acid groups to the MWCNT [31].

Both pristine WBPU and WBPU/*f*-MWCNT nanocomposite dispersions were prepared using the prepolymer mixing method (see Scheme 1) following our previous report [13]. The compositions are summarized in Table 2. The moles of Poly(tetramethyleneoxide glycol) (PTMG), poly(ethylene glycol) (PEG), dimethylolpropionic acid (DMPA), triethylamine (TEA), 4,4-dicyclohexylmethane diisocyanate ($H_{12}$MDI) and ethylenediamine (EDA) were maintained constant, whereas the *f*-MWCNT content was increased up to 2.5 wt%. However, above 2.0 wt% *f*-MWCNTs, the WBPU/*f*-MWCNT nanocomposite dispersions were unstable; therefore, dispersions loaded above 2.0 wt% *f*-MWCNTs were not considered as coating materials in this study. The mentioned composition provided same hard segment, soft segment and carboxyl salt

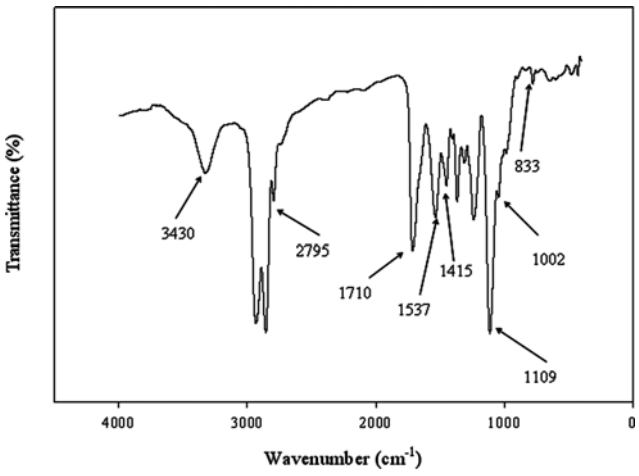


**Fig. 2. FT-IR spectrum of pristine WBPU coating.**

group contents for all of the coating materials. The solid content remained constant at 30 wt%. The pristine WBPU and WBPU/*f*-MWCNT nanocomposite coatings were identified by characteristic IR peaks (see Fig. 2), such as the N-H peak and the C=O peak. Peaks at 1,710 $cm^{-1}$ and 3,430 $cm^{-1}$ appeared for the C=O and N-H groups, respectively [14]. The spectra were also characterized by the bands at 2,800-3,000 $cm^{-1}$, 2,795 $cm^{-1}$ and 1,109 $cm^{-1}$, which correspond to CH, O-$CH_2$ and C-O-C stretching and the ether group, respectively. The band at 1,415 $cm^{-1}$ is attributed to $CH_2$ scissoring and $CH_3$ deformation, whereas the absorbance's at 1,002 and 1,012 $cm^{-1}$ are attributed to the stretching and rocking vibrations of the C-C and $CH_2$ groups, respectively. A very weak single band observed at 833 $cm^{-1}$ is attributed to either the coupled vibrations of the C-O stretching or $CH_2$ rocking modes [14]. A strong

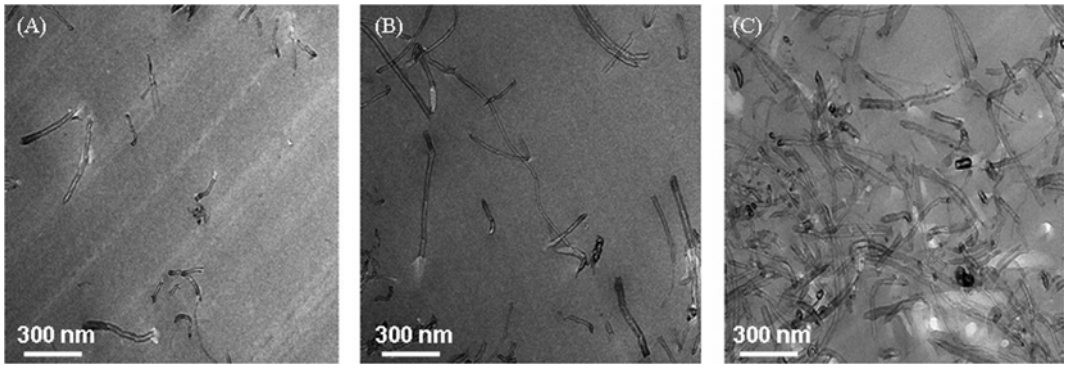


**Fig. 3. TEM microphotographs of WBPU/*f*-MWCNT coatings with different *f*-MWCNT content (A) 0.5 wt% (B) 1.0 wt% and (C) 2.0 wt%.**

band assigned to the asymmetric stretching vibration of the C-N group is expected at 1,040 $cm^{-1}$; however, this band overlaps with the very strong band at 1,109 $cm^{-1}$, corresponding to the C-O-C stretching vibration of the ether groups in the PU films. However, there was no difference recorded between the pristine WBPU and WBPU/*f*-MWCNT coatings. To assess the dispersion of *f*-MWCNTs in the coatings, TEM analysis was conducted. A typical TEM image is shown in Fig. 3, which clearly shows that the *f*-MWCNTs are dispersed homogeneously in the PU matrix. No agglomeration was observed for any of the coatings. The homogeneously dispersed *f*-MWCNTs might be acted as reinforcement in coatings [13,30].

A higher level of water resistance is a prerequisite for coatings applied for corrosion protection [14,30]. Typically, the water resistance of a coating is assessed by its water contact angle and water absorption (%) [30]. The effects of *f*-MWCNT content on the water contact angle and water absorption (%) are shown in Fig. 4. The water contact angle and water absorption (%) were both found to vary with *f*-MWCNT content; the water contact angle increased with increasing *f*-MWCNT content, whereas the water absorption (%) decreased with increasing *f*-MWCNT content. This result implies that the coating hydrophobicity increased with increasing *f*-MWCNT content [30]. Furthermore, this result suggests that the *f*-MWCNTs act as a barrier for passing water and air. The highest water contact angle and lowest water absorption (%) of the coating confirmed the highest resistance for the coating containing 2.0 wt% *f*-MWCNTs.

Bare and coated mild steels were exposed and monitored visually under defined intervals (see Fig. 5). For bare mild steel, the first stage of corrosion began very quickly, as some pits were observed within four days. The pristine WBPU coating showed slight protection, as there was no pitting observed over 15 days, after which time some pits were observed. This observation indicates that the pristine coating had already degraded within those 15 days. The pit density increased gradually with time, covering the entire coating in the following 15 days. Different results were observed for the composite coatings. The protection efficiency significantly improved upon using the WBPU/*f*-MWCNT coatings. After 90 days, the extent of damage attributed to corrosion was much greater in the pristine WBPU coating compared to the WBPU/*f*-MWCNT nanocomposite coatings. Corrosion affected more than half of the coating area of the pristine WBPU coating, whereas the extent of deterioration was much less for the nanocomposite coatings, par-

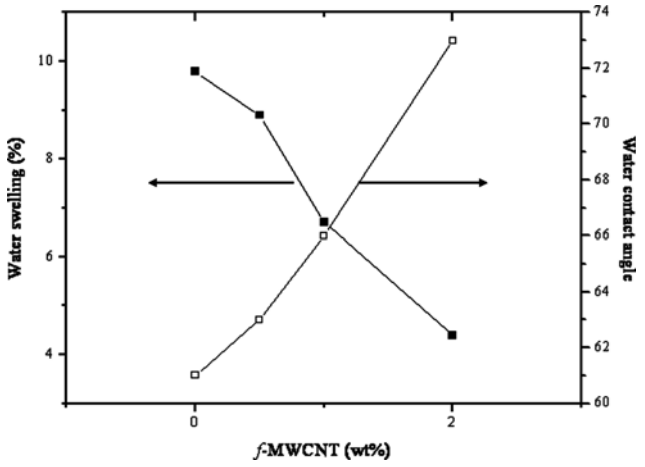


**Fig. 4. Effect of f-MWCNT content on water swelling and water contact angle.**

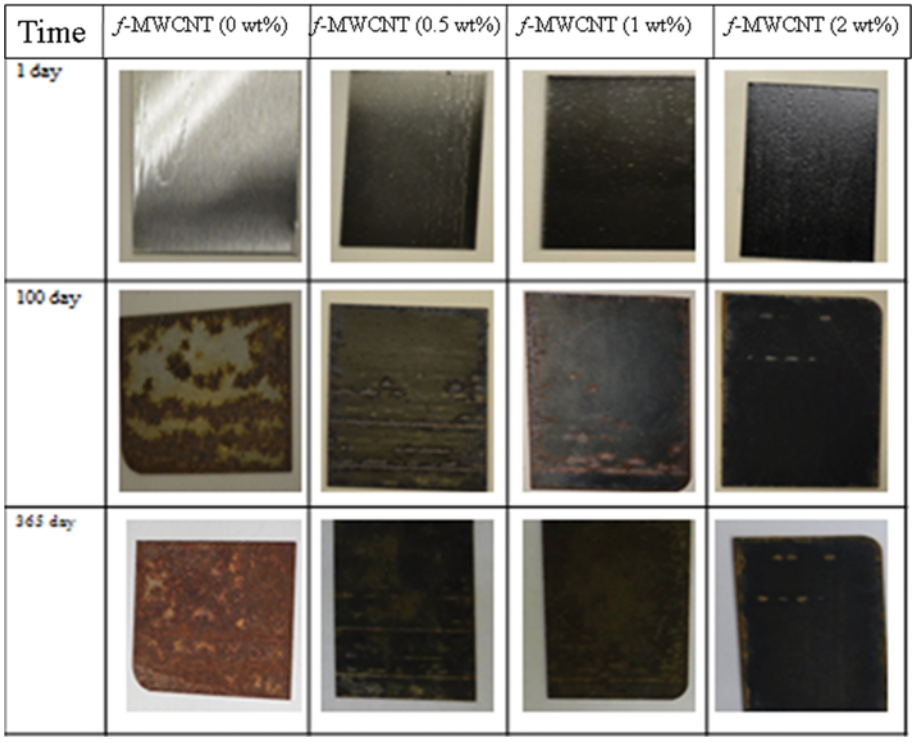


**Fig. 5. Exposed coatings under sunlight.**

ticularly for those with increased concentrations of *f*-MWCNTs up to 2.0 wt%. After 365 days, the final inspection determined that the specimen using the pristine WBPU coating was fully damaged. The specimen using the WBPU/*f*-MWCNT nanocomposite coating containing 2.0 wt% *f*-MWCNTs was still very much intact, whereas the coating with 1.0% *f*-MWCNTs was considerably damaged. Therefore, the incorporation of *f*-MWCNTs into the WBPU coating enhanced its degradation and corrosion resistance and the maximum protection was observed with a *f*-MWCNT content of 2.0 wt%.

To justify the visual inspection of the coatings, potentiodynamic polarization (PDP) was conducted for all (exposed and unexposed) of the coatings, except the exposed pristine WBPU coating which has been completely damaged at exposed condition. Fig. 6 presents the potentiodynamic polarization (PDP) curves for all the coatings. This analysis showed that all WBPU/*f*-MWCNT unexposed coatings lead to better protection of the mild steel compared with the pristine unexposed WBPU coating. Coatings containing *f*-MWCNTs were observed to exhibit lower levels of $i_{corr}$ (see Fig. 6) compared to the pristine WBPU coating, which indicated that the incorporation of *f*-MWCNTs into the coating increased the corrosion resistance of the composite coating. It was also determined that an increase in the *f*-MWCNT content resulted in a decrease in $i_{corr}$ for the WBPU/*f*-MWCNT coatings, implying increasing corrosion protection efficiency with increasing *f*-MWCNT loading of the coating. However, the rate of decreasing of $i_{corr}$ value with increasing *f*-MWCNT content was not the same. Initially the $i_{corr}$ value increased slightly with addition of *f*-MWCNT content. However, the $i_{corr}$ value increased significantly with addition of 2.0 wt% *f*-MWCNT content. It has been reported elsewhere [32] that the corrosion protection of polymer/CNT coatings highly depends on the changed microstructure of the dispersed CNTs. The corrosion protection decreased if micro pores were created in the coatings by the loading of CNTs, which led to the comparatively easy passing of electrolyte through the coating [32]. However, if the CNTs can act as a barrier or increase the surface hydrophobicity, they will resist the electrolyte passing through the coating, resulting in higher corrosion protection [32]. Moreover, the CNTs can act as a UV absorber and reduce coating degradation [33]. In this study, the latter reason might be active in the unexposed coatings, showing higher corrosion protection efficiency of the WBPU/*f*-MWCNT coatings. This interesting result was obtained when the exposed coatings were analyzed. All of the $i_{corr}$ values (see Fig. 6) increased with time when compared to their respective unexposed coatings. The fact is that the $i_{corr}$ values changed at a different rate with different *f*-MWCNT content even after exposure for 365 days. This result also implies that all of the coatings suffered from degradation at different rate. However, the $i_{corr}$ value (see Fig. 6) increased to a lesser extent with higher *f*-MWCNT content, implying that the least damaged coatings contained higher *f*-MWCNT contents. In this case, the *f*-MWCNTs might act as a UV absorber, reducing coating degradation [33].

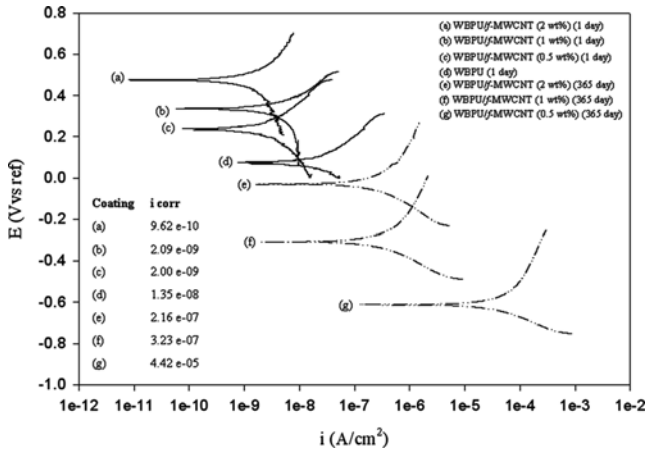


**Fig. 6. Polarization curves of exposed coatings with different *f*-MWCNT content.**

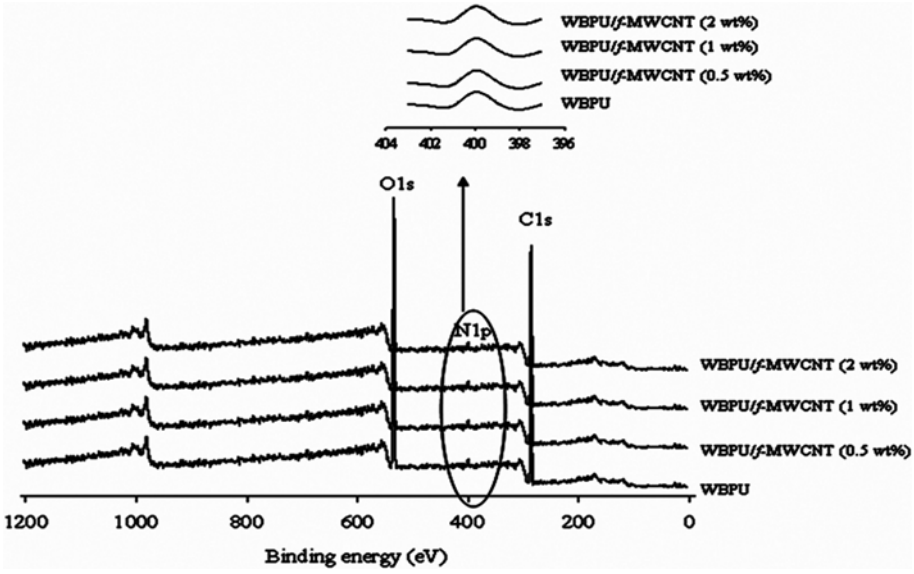


**Fig. 7. XPS spectra of WBPU films with different *f*-MWCNT content.**

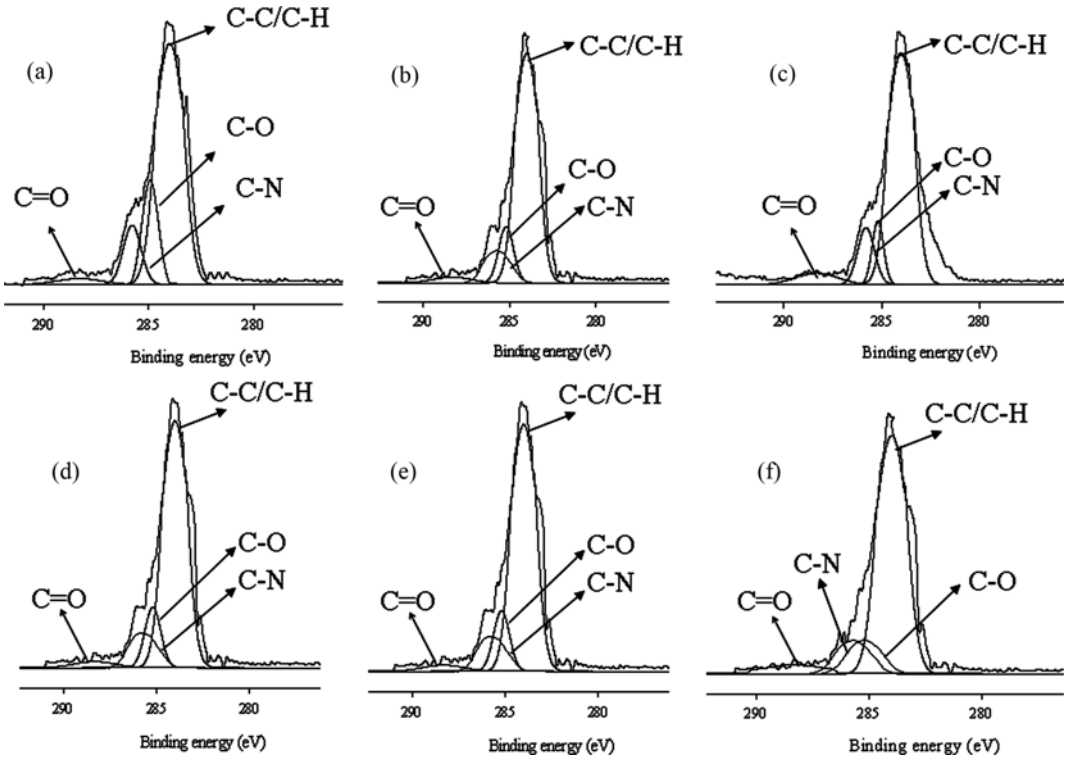


**Fig. 8. Curve fitting of XPS C1s core level spectra of coatings: (a) *f*-MWCNT 0 wt% before exposed, (b) *f*-MWCNT 2 wt% before exposed, (c) *f*-MWCNT 0 wt% after exposed 90 day, (d) *f*-MWCNT 2 wt% after exposed 90 day, (e) *f*-MWCNT 2 wt% after exposed 200 day, (f) *f*-MWCNT 2 wt% after exposed 365 day.**

The top surfaces of all the coatings were analyzed using XPS. The peaks for certain atoms were found to be nearly identical in all coatings (see Fig. 7). The peaks at 531, 285 and 400 eV attributed to oxygen (1s), carbon (1s), and nitrogen (1p), respectively, were observed in the survey spectra for all the coatings. Because the oxygen (1s), carbon (1s), and nitrogen (1p) atoms have different binding energies, their peaks are observed at different values. However, for the carbon atoms in different environments with different functional groups, the C1s binding energies of these functional groups are very close to each other and their original functional groups can be determined using the curve fitting analysis. The C1s peaks are classified into four groups: the C=O carbon atom appearing at 289.7-285.8 eV, the C-C or C-H at 282.0-285.9 eV, the C-O at 284.1-286.1 eV and the C-N at 284.5-287.1 eV (see Fig. 8). With the inclusion of *f*-MWCNTs, the area at 289.7-285.8 eV (for the carbonyl groups) decreased (see Fig. 9). It has been reported elsewhere that the carbonyl contribution is attributed to the urethane/urea groups of WBPU [33]. The smaller carbonyl area implies a lower content of urethane/urea groups on the surface. The lowest carbonyl area was found for the highest 2.0 wt% *f*-MWCNT content (see Fig. 9), implying that the maximum amount of buried urethane/urea groups by *f*-MWCNTs on the surface was found at this composition.

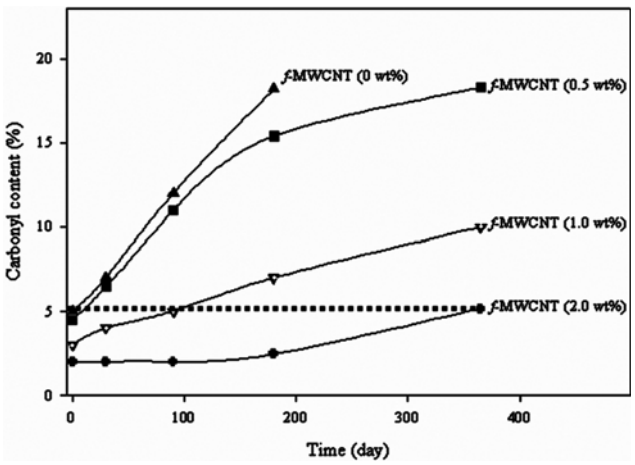


**Fig. 9. Carbonyl content of exposed coatings after certain interval.**

The coatings exposed to open air atmosphere are susceptible to degradation, leading to eventual corrosion of the mild steel. It has been reported [34,35] that carbon dioxide and carbon monoxide are two prominent degrading, oxidized products, which can be detected by the presence of carbonyl groups through XPS analysis. The increased carbonyl content of exposed coatings also implies less efficient corrosion protection of the coatings. The carbonyl content of all the exposed coatings is shown in Fig. 9. The carbonyl content changed significantly for the pristine WBPU exposed coating, which further increased with time. The carbonyl content changed from 5% to 12% after 90 days (see Fig. 9), implying significant degradation of the coating. This degradation resulted in the facile passing of water/air through the coating into the mild steel and directly impacted the corrosion protection of the coating. Very low corrosion protection was observed in this case. However, the car-

bonyl content was different when 1.0 wt% or higher *f*-MWCNT content was used in the coatings. The carbonyl content was observed to be lowest for the WBPU/*f*-MWCNT coating with 2.0 wt% of *f*-MWCNT content (see Fig. 9). This result can be ascribed to the lowest chain scission of urethane/urea groups in the presence of UV (sunlight). Herein, the *f*-MWCNTs acted as a UV absorber, which protected the chain scission of urethane/urea groups, eventually decreasing the degradation of the coating. Hence, the mild steel was also protected from corrosion.

## CONCLUSIONS

All of the prepared dispersions were coated on mild steel and exposed to natural weather conditions for 365 days. All of the coatings had a tendency to degrade under these conditions. The degradation decreased with inclusion of *f*-MWCNTs, which further decreased with increasing *f*-MWCNT content. The dispersed *f*-MWCNTs acted as both a barrier (before exposure) and UV absorber (during exposed) in the WBPU/*f*-MWCNT coatings. A combination of these two factors improved the overall protection of the coatings for a moderate length of time. The protection can be further improved by tuning the monomers and their contents. Over the last decade, the restriction of organic solvents and toxic inhibitors has created a significant challenge to the coating industry. The findings reported herein open a new door for the protection of metals in an environmentally friendly way.

## ACKNOWLEDGEMENT

This study was supported by Center of Research Excellence in Corrosion (CoRE-C), King Fahd University of Petroleum and Minerals (KFUPM), Dhahran 31261, Saudi Arabia.

## REFERENCES

1. D. K. Chattopadhyay and K. V. S. N. Raju, *Prog Polym. Sci.*, **32**, 352 (2007).
2. M. M. Rahman, A. Hasneen, Y. K. Lee and K. T. Lim, *J. Sol Gel. Sci. Technol.*, **67**, 473 (2013).
3. G. N. Chen and K. N. Chen, *J. Appl. Polym. Sci.*, **63**, 1609 (1997).
4. F. M. B. Coutinho and M. C. Delpech, *Polym. Degr.*, **70**, 49 (2000).
5. M. M. Rahman, H. D. Kim and W. K. Lee, *Fib. Pol.*, **10**, 6 (2009).
6. M. de. Meijer, *Prog. Org. Coat.*, **43**, 217 (2001).
7. L. Podgorski and J. M. Roux, *Surf. Coat. Int.*, **82**, 590 (1999).
8. M. V. Cristea, B. Riedl and P. Blanchet, *Prog. Org. Coat.*, **72**, 755 (2011).
9. M. S. Lowry, D. R. Hubble, A. L. Wressell, M. S. Vratsanos, F. R. Pepe and C. R. Hegedus, *J. Coat. Technol. Res.*, **5**, 233 (2008).
10. M. Rashvand, Z. Ranjbar and S. Rastegar, *Prog. Org. Coat.*, **71**, 362 (2011).
11. F. Gugumus, *Polym. Degrad. Stab.*, **39**, 117 (1993).
12. P. V. Yaneff, K. Adamsons, N. Cliff and M. Kanouni, *J. Coat. Technol. Res.*, **3**, 201 (2004).
13. M. M. Rahman, E. Y. Kim, K. T. Lim and W. K. Lee, *J. Adhesion Sci. Technol.*, **23**, 839 (2009).
14. M. M. Rahman and H. D. Kim, *J. Adhesion Sci. Technol.*, **21**, 81 (2007).
15. M. L. Zheludkevich, I. M. Salvado and M. G. S. Ferreira, *J. Mater. Chem.*, **15**, 5099 (2005).
16. A. Cook, A. Gabriel and N. Laycock, *J. Electro. Chem. Soc.,* **151**, 529 (2004).
17. R. Suleiman, M. M. Rahman, N. Alfaifi, B. El. Ali and R. Akid, *Corrosion Engin. Sci. Technol.*, **48**, 525 (2013).
18. X. Shi, T. A. Nguyen, Z. Y. Liu and R. Avci, *Surf. Coat. Technol.*, **204**, 237 (2009).
19. T. L. Metroke, O. Kachurina and E. T. Knobbe, *Prog. Org. Coat.*, **44**, 295 (2002).
20. T. L. Metroke, O. Kachurina and E. T. Knobbe, *Prog. Org. Coat.*, **44**, 185 (2002).
21. T. L. Metroke, J. S. Gandhi and A. Apblett, *Prog. Org. Coat.*, **50**, 231 (2004).
22. T. L. Metroke and A. Apblett, *Prog. Org. Coat.*, **51**, 36 (2004).
23. M. Behzadnasab, S. M. Mirabedini, K. Kabiri and S. Jamali, *Corrosion Sci.*, **53**, 89 (2011).
24. P. J. Kinlen, Y. Ding and D. C. Silverman, *Corrosion*, **58**, 490 (2002).
25. G. Markevicius, S. Chaudhuri, C. Bajracharya, R. Rastogi, J. Xiao, C. Burnett and T. Q. Chastek, *Prog. Org. Coat.*, **75**, 319 (2012).
26. J. F. Shen, W. S. Huang, L. P. Wu, Y. Z. Hu and M. X. Ye, *Composites Sci. Technol.*, **67**, 3041 (2007).
27. L. Liu and J. C. Grunlan, *Adv. Funct. Mater.*, **17**, 2343 (2007).
28. L. Böger, M. H. G. Wichmann, L. O. Meyer and K. Schulte, *Composites Sci. Technol.,* **68**, 1886 (2008).
29. B. K. Kim, J. W. Seo and H. M. Jeong, *Europ. Polym. J.,* **39**, 85 (2003).
30. J. Y. Kwon and H. D. Kim, *J. Appl. Polym. Sci.*, **96**, 595 (2005).
31. D. Robati, S. Bagheriyan and M. Rajabi, *Int. Nano Lett.*, **5**, 179 (2015).
32. F. Batmanghelich and M. Ghorbani, *Ceram. International*, **39**, 5393 (2013).
33. M. M. Rahman, H. H. Chun and H. J. Park, *Coat. Tech. Res.*, **8**, 389 (2011).
34. L. F. Chun, H. Y. Sheng, W. Z. Yu, S. H. Wei, H. E. Hou and K. E. Wei, *Chin. Sci. Bull.*, **55**, 650 (2010).
35. R. Asmatulu, R. O. Claus, J. B. Mecham and S. G. Corcoran, *Mater. Sci.*, **43**, 415 (2007).